Quantitative Analysis of Regional Wall Motion by Gated Myocardial Positron Emission Tomography: Validation and Comparison with Left Ventriculography

Keiji Yamashita, Nagara Tamaki, Yoshiharu Yonekura, Hiroshi Ohtani, Hideo Saji, Takao Mukai, Hirofumi Kambara, Chuichi Kawai, Toshihiko Ban, and Junji Konishi

Department of Radiology and Nuclear Medicine, The 3rd Division, Department of Internal Medicine, Department of Cardiovascular Surgery, Kyoto University, School of Medicine

Electrocardiographically gated positron emission tomography (ECG-gated PET) with [^{13}N] ammonia was used to assess regional myocardial wall motion of left ventricle (LV) based on a nongeometric method in nine healthy volunteers and 16 patients with coronary artery disease (CAD). Three transverse sections (upper, middle, and lower) with 16-mm intervals at end-diastole (ED) and end-systole (ES) were analyzed. The LV wall was divided into eight segments with every 30 degrees from septal wall to lateral wall. Based on circumferential profile analysis, the percent count increase ({ES count − ED count} ÷ ED count × 100) in each segment was analyzed as an index of regional wall motion. In the study of normal controls, the percent count increase was the lowest (32.9 ± 7.2%) at septal wall of the lower slice and the highest (72.8 ± 26.5%) at lateral wall of the upper slice ($p < 0.01$). In five normal controls, the percent count increase was compared with the percent systolic wall thickening analyzed by magnetic resonance imaging, and a good correlation was observed ($r = 0.84$). In the study of patients with CAD, the percent count increase was compared with wall motion assessed by left ventriculography (LVG). The percent count increase significantly decreased as wall motion on LVG worsened. In addition, the value in normal controls tended to be higher than that in the segments with normal wall motion in patients with CAD. Thus, quantitative analysis of regional wall thickening was feasible by ECG-gated PET, which should be useful for combined analysis of regional function, perfusion and metabolism in patients with CAD.

J Nucl Med 30:1775–1786, 1989

Positron emission tomography (PET) is an excellent means for assessing regional blood flow and metabolism in vivo. In the cardiac study, PET has been used for the detection of myocardial ischemia (*1–8*), identification of tissue viability (*1,5,9–12*) and pathophysiologic assessment of various cardiac diseases (*13*). However, most of these analyses have been undertaken with nongated acquisition. Recently, in PET studies, electrocardiographically (ECG) gated acquisition has been available, which permits combined analysis of regional cardiac function, perfusion and metabolism (*14*).

Based on the principle of partial volume effect on PET images (*15*), regional myocardial count correlates with the wall thickness when it is less than twice of the spatial resolution in full width at half maximum (FWHM). Previously, systolic count increase from end-diastole (ED) to end-systole (ES) was analyzed as systolic wall thickening using animals (*16*). However, there have been no such studies dealing with men. We analyzed the percent count increase of left ventricle (LV) by ECG-gated PET as an index of wall thickening in normal control and patients with coronary artery disease (CAD).

The purpose of this study is to establish quantitative assessment of systolic count increase by ECG-gated PET and to evaluate its reliability by comparing it with wall motion assessed by conventional left ventriculography (LVG).

Received Dec. 6, 1988; revision accepted June 27, 1989.

For reprints contact: Keiji Yamashita, MD, Dept. of Radiology and Nuclear Medicine, Kyoto University Medical School, Sakyo-ku, Kyoto, 606, Japan.

PATIENTS AND METHODS

Normal Control and Patients Population

Nine healthy volunteers were selected as normal controls. They were all men (age range 31–70 yr, mean 52.3) with normal blood pressure and had no abnormality on ECG, no cardiac symptoms, nor other medical problems.

Sixteen clinically stable patients with CAD (all men), aged 48–64 yr (mean 57.8 yr) were selected for this study. Fifteen patients had myocardial infarction (MI) and one patient had angina pectoris. Location of MI was documented by ECG findings (Table 1). Fifteen patients had significant coronary artery stenosis (≧75% stenosis) on coronary arteriography but one patient had no significant stenosis. Those with marked LV hypertrophy on ECG were excluded in this analysis. The interval from the onset of MI ranged from 2 mo to 10 yr (mean 20.8 mo). Four patients had septal MI, 12 had anterior MI including four extensive anterior MI, two had inferior MI and two had apical MI, respectively (MI was seen at two regions in four patients). ECG gated PET and LVG were performed within 2 wk and no change in symptom or ECG was observed between two examinations. All of them gave a written informed consent.

ECG-gated PET

ECG-gated PET was performed using a whole-body, multislice PET scanner (Positologica III; Hitachi Medical Corporation, Tokyo) (*17*). This scanner has four continuously rotating rings providing seven tomographic sections with 16 mm intervals. The spatial resolution was 7.6 mm in full width at half maximum (FWHM) of a line source at the center of the field. The effective resolution in a reconstructed image (128 × 128 matrices) with a Shepp-Logan filter convoluted with 2-mm sigma Gaussian was ~9 mm in FWHM. The axial resolution was 12 mm in FWHM at the center of the field (*17*).

A small cyclotron (SYPRIS 325; Sumitomo Heavy Industry, Tokyo) was used for production of [^{13}N]ammonia. It was produced by $^{16}O(p, \alpha)^{13}N$ nuclear reaction with water irradiation, followed by a reduction to [^{13}N]ammonia with titanous hydroxide (*6–7*).

A transmission scan was performed for 15 min before the administration of the labeled compounds using a rotating germanium-68/gallium-68 standard plate source for measuring attenuation factor. The position was marked with a felt pen on the patient's chest and was aligned with a light beam. A resting emission scan was obtained 10 min following the intravenous injection of 10–20 mCi of [^{13}N]ammonia in an ECG-gated mode. The ECG-gating signal directed the incoming data. Data were collected for 1000–1200 beats (15–20 min). ED was defined as the 50–80 msec period following R-wave of ECG and ES as the period of same duration following downslope of T-wave. Each image of ED and ES includes 1 to 3 × 10^5 counts. The data were acquired in 128 × 128 matrices (matrix size was 2.5 × 2.5 mm). Seven transverse slices of left ventricle at both ED and ES were obtained with 16-mm intervals.

Image Analysis of ECG-Gated PET

Two experimental observers performed image analysis of PET independently without knowing patient's information. Each observer performed the analysis two times.

From seven transverse sections of LV myocardium at ED displayed on a CRT monitor, middle slice where LV chamber size was maximum was determined and three slices (the upper,

TABLE 1
Patients List

Patient no.	Age (yr)	Sex	Site of MI	Interval from MI	Coronary artery stenosis (≧75%)	Wall motion by biplane (RAO and LAO) LVG
1	64	M	Angina pectoris	—	3VD	Normal
2	53	M	Ant, Sep	5 mo	LAD,CX	AL,AX:Rd SP:Ak
3	58	M	Inf	4 mo	3VD	AL,AX SP:Rd DP,PB,PL:Ak
4	55	M	extensive-Ant	2 mo	LAD	AB:Rd AL,AX,SP:Dy
5	59	M	Ant, Sep	6 mo	LAD	AB:Rd AL,AX:Ak
6	60	M	Apex	2 mo	LAD	AL,DP:Rd AX,SP:Dy
7	58	M	Ant, Sep	9 mo	LAD,CX	AL,DP,SP,PL:Rd AX:Ak
8	58	M	Ant, Sep	5 mo	LAD,CX	AX,DP,SP:Rd AL,PL:Ak
9	60	M	Ant	8 yr	3VD	AB,DP,PB:Rd AL:Ak Ax:Dy
10	58	M	extensive-Ant	1 yr	3VD	AL,SP:Rd DP,PB,PL:Ak AX:Dy
11	62	M	Apex	8 mo	LAD,CX	DP,SP:Dy
12	55	M	Ant	5 mo	LAD,CX	AL,SP:Rd
13	55	M	Ant	2 mo	LAD,CX	AX,DP:Rd AL,SP:Ak
14	48	M	extensive-Ant	10 yr	3VD	AL,DP,PB,SP:Rd AX:Ak
15	60	M	Ant, Inf	1 yr	no significant stenosis	AL,AX,PB,SP:Rd
16	61	M	extensive-Ant	2 yr	3VD	AL,DP,PB,SP:Rd AX,PL:Ak

MI = myocardial infarction; LVG = left ventriculography; RAO = 30° right anterior oblique projection; LAO = 30° left anterior oblique projection; Ant = anterior wall; Sep = septal wall; Inf = inferior wall; 3VD = three vessels disease; LAD = left anterior descending artery; CX = circumflex artery.

Based on AHA criteria (*17*), RAO view of LVG was divided into anterobasal (AB), anterolateral (AL), apical (AX), diaphragmatic (DP) and posterobasal (PB) segments. LAO view of LVG was divided into septal (SP) and posterolateral (PL) segments. Wall motion by LVG was analyzed semiquantitatively as normal (Np), reduced (Rd), akinesis (Ak) and dyskinesis (Dy).

middle and lower) with 16-mm intervals were selected for analysis. When LV lumen was not seen clearly (especially at ES), such slices were excluded (in normal control, three of nine upper slices were excluded; in patients with CAD, three of 16 upper slices and one of 16 lower slices were excluded). Then, matrices of these images were reduced into 64 × 64 (matrix size was 5 × 5 mm). Parallel line to septal wall was regarded as long axis and vertical line as short axis in each slice (Fig. 1A). Mid-point of these two lines was determined as LV center. The external and internal area of LV wall were excluded from analysis (Fig. 1A). Five-point averaging (covering about 25 mm thickness) circumferential profile analysis was performed at every six degrees around the center point (Fig. 1B). Then, the LV wall was divided into 12 segments (each including five circumferential radial lines) with every 30 degrees (Fig. 1C). Eight segments excluding basal ones were selected for analysis. Segments of each slice were numbered in order from 1: septal wall to 8: lateral wall (Fig. 1C). When posterior wall was clearly seen (it was seen at lower slice in many cases), it was also analyzed (Fig. 1C). Mean count was calculated from five circumferential points by the segment at both ED and ES.

Comparison with Magnetic Resonance Imaging

In five of the normal controls, magnetic resonance imaging (MRI) was performed using a superconducting magnet operating at 1.5 Tesla (General Electric, Milwaukee, WI). The imaging matrix was 256 × 256, signal acquisition was two times, repetition time was R-R interval of ECG, and echo time was 25/50 msec. ED was defined as R-wave of ECG and ES was as down slope of T-wave. Corresponding to PET slices, two transverse slices of 5-mm thickness were obtained with 16-mm intervals at ED and ES. Eight segments were determined as same as PET (totally 80 segments) and compared with ECG-gated PET.

Evaluation of LVG

LVG was performed in 30-degree right anterior oblique (RAO) and 60-degree left anterior oblique (LAO) projections, based on AHA criteria (*18*). LV wall was divided into anterobasal, anterolateral, apical, diaphragmatic and posterobasal segments in RAO view and septal and posterolateral segments in LAO view images.

Three experienced observers visually assessed the regional wall motion of LVG independently without knowing the results of ECG-gated PET nor other clinical informations and classified it independently as normal, reduced, akinesis and dyskinesis (including aneurysmal). When the judgment of two or three observers was coincident, it was adopted. When the judgment of three observers was different from each other, the medium of three judgments was adopted. However, there were no such cases.

Analysis of Normal Control in PET

In normal control, three parameters were calculated in each segment; the percent ED count (by defining the maximum count in ED segments as 100% in each slice), the percent ES count (same as the former) and the percent count increase. The percent ED count and the percent ES count was calculated as follows:

$$\text{Percent ED count} = \frac{\text{ED count in each segment}}{\text{ED maximum count}} \times 100(\%)$$

$$\text{Percent ES count} = \frac{\text{ES count in each segment}}{\text{ED maximum count}} \times 100(\%)$$

The percent count increase was calculated as follows:

$$\text{Percent count increase} = \frac{\text{ES count} - \text{ED count}}{\text{ED count}} \times 100(\%).$$

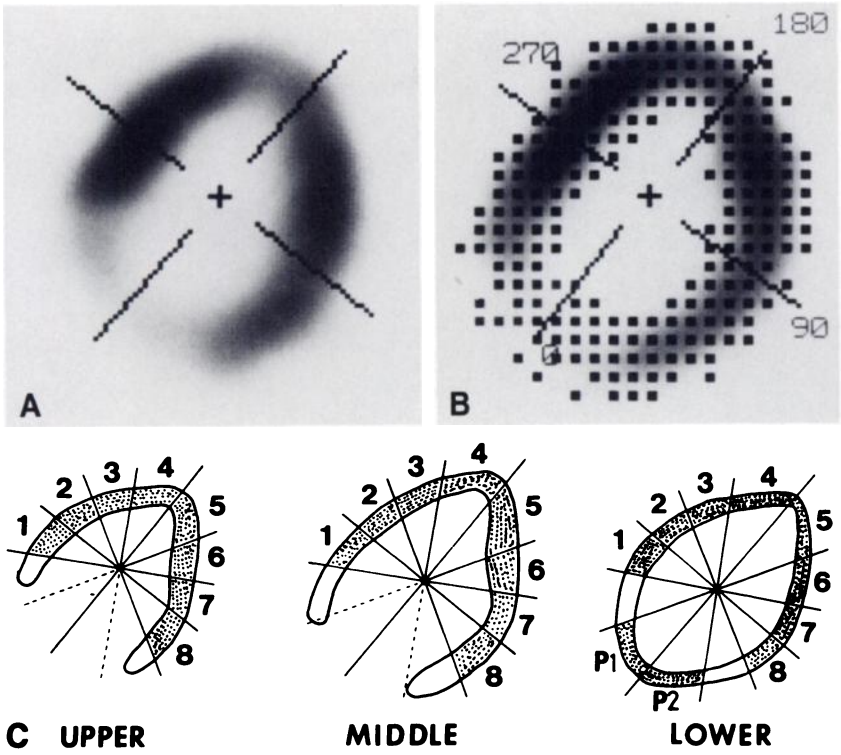

FIGURE 1
A: Parallel line to septal wall was regarded as long axis and vertical line as short axis. The mid-point of both two lines were determined as center point in each slice. Range was determined to exclude inner and outer area of left ventricular wall. B: Five-point averaging circumferential profile analysis (covering 25-mm thickness) was performed every six degrees. C: Left ventricular wall was divided into eight segments with every 30 degrees numbered in order from septal wall to lateral wall. When posterior wall (P_1, P_2) was clearly seen, it was also analyzed.

The percent ED count was considered to represent perfusion × ED wall thickness. The percent ES count was considered to represent percent ED count × percent wall thickening. The percent count increase was considered to be in proportion to the percent wall thickening and was selected as an index of regional systolic wall thickening.

Analysis of Normal Control in MR Imaging

ED and ES wall thickness was measured in each segment. When thickness was different in one segment, average value was adopted. In MR imaging, the percent systolic wall thickening was calculated as follows:

$$\text{Percent wall thickening} = \frac{\text{ES thickness} - \text{ED thickness}}{\text{ED thickness}} \times 100\ (\%).$$

The percent wall thickening assessed by MR imaging was compared with the percent count increase assessed by ECG-gated PET.

Analysis of Patients

In patients with CAD, the percent count increase was compared with regional wall motion assessed by LVG. Segment 4–5 of the upper slice of ECG-gated PET was regarded as anterobasal wall of LVG, segment 4–5 of the middle slice as anterolateral, segment 4–5 of the lower slice as apical, segment P_1–P_2 as posterobasal, segment 1–2 of the middle slice as septal and segment 7–8 of the middle slice as posterolateral, respectively (Fig. 1C). However, diaphragmatic wall was excluded for analysis because this segment was not clearly visualized in the transverse section.

Statistical Analysis

Each value was expressed as mean ± s.d. The regional differences in the percent ED count, the percent ES count and the percent count increase of normal control were compared using analysis of variance. In patients with CAD, the differences of the percent count increase in various wall motion assessed by LVG were analyzed using paired t-test. The significant level was considered as $p < 0.05$ in both analysis of variance and paired t-test.

RESULTS

ECG-Gated PET in Normal Control

Figure 2 shows ED and ES images of the upper, middle, and lower slices of a normal case. The count increased from ED to ES as the LV chamber size decreased. Figure 3 and Table 2 show the percent ED count, the percent ES count and the percent count increase in normal control. Among nine normal cases, posterior wall (P_1, P_2) was clearly seen in seven cases (it was seen at a lower slice in all 7 cases).

The percent ED count in various segments was significally different ($p < 0.001$). The percent ED count ranged from 69.9 ± 7.3% (segment 4 of the lower slice) to 93.3 ± 7.6% (segment 1 of upper slice). In all slices, the percent ED count in anterior wall or apex was significantly lower than that in septal wall and anterolateral wall. In the upper and middle slices, the percent ED count in septal wall was significantly higher than that in lateral wall. (Fig. 3A, Table 2A)

The percent ES count in various segments was significantly different ($p < 0.01$). The percent ES count ranged from 120.1 ± 13.7% (segment 4 of the lower slice) to 143.8 ± 7.4% (segment 7 of the upper slice). In the upper and lower slices, the percent ES count in anterior wall or apex was significantly lower than that in lateral wall. In the upper slice, the percent ES count in septal wall was significantly lower than that in lateral wall. However, these differences were relatively minimal in comparison with the percent ED count. (Fig. 3B, Table 2B)

The percent count increase in various segments was

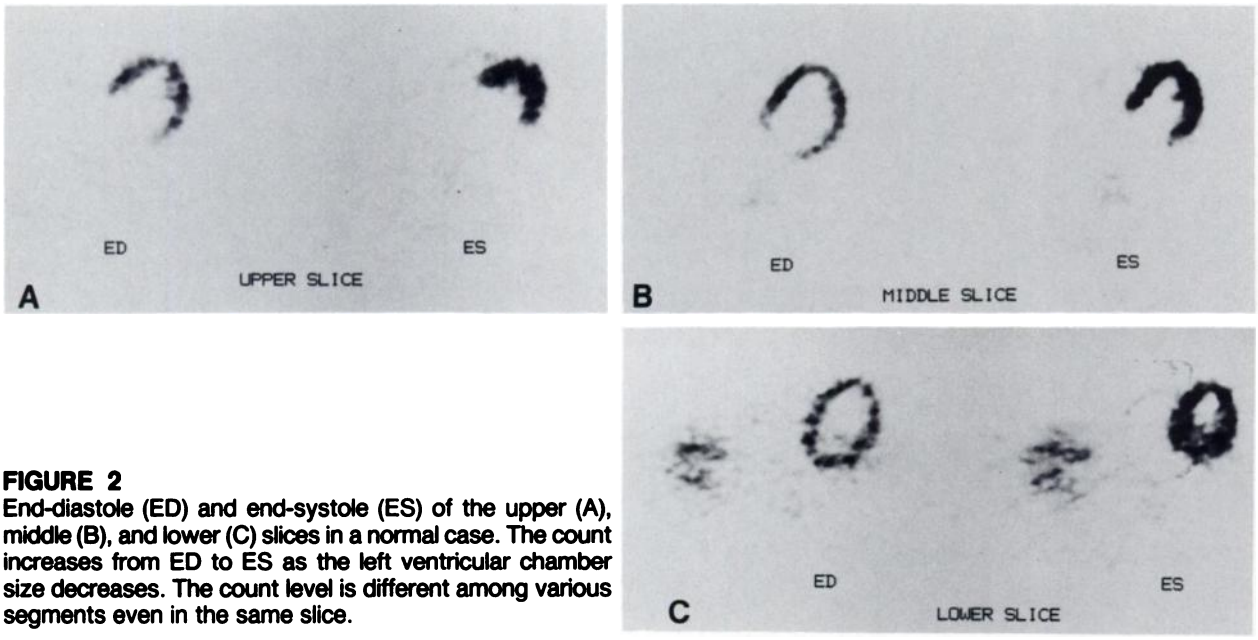

FIGURE 2
End-diastole (ED) and end-systole (ES) of the upper (A), middle (B), and lower (C) slices in a normal case. The count increases from ED to ES as the left ventricular chamber size decreases. The count level is different among various segments even in the same slice.

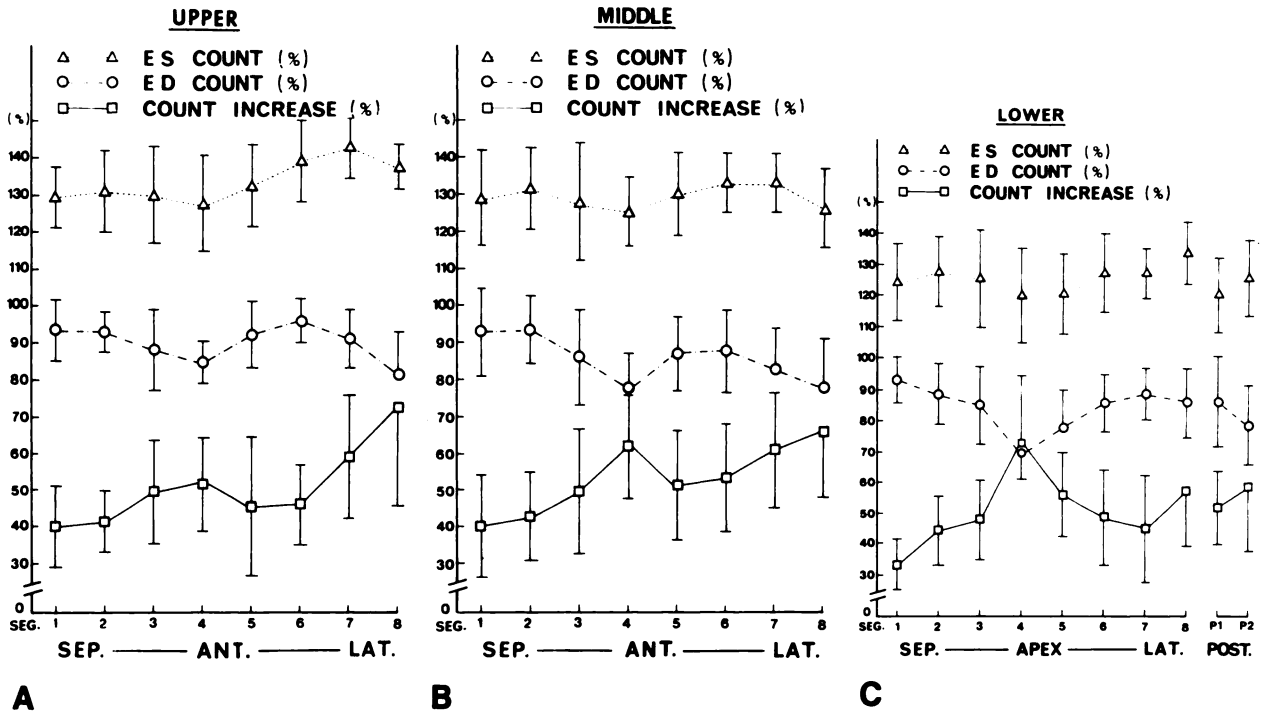

FIGURE 3
The percent ED count, the percent ES count and the percent count increase in the upper (A), middle (B), and lower slices (C) of nine normal cases are shown. Values are mean ± s.d. The percent ED count of anterior (or apex) and lateral wall were significantly lower than that of septal and anterolateral wall. The percent ES count was relatively constant compared with the percent ED count. The percent count increase of anterior (or apex) and lateral wall were significantly higher than that of septal and anterolateral wall in opposition to the percent ED count.

significantly different ($p < 0.001$). The percent count increase ranged from 32.9 ± 7.2% (segment 1 of the lower slice) to 72.8 ± 26.5% (segment 8 of the upper slice). In the middle and lower slices, the percent count increase in anterior wall or apex was significantly higher than that in septal wall. In all slices, the percent count increase in lateral wall was significantly higher than that in septal wall. In the lower slice, the percent count

TABLE 2A
The Percent ED Count in Normal Control (%)

Slice/segment	1	2	3	4	5	6	7	8
Upper slice	93.3 ± 7.6	92.7 ± 4.5	88.2 ± 10.3	84.7 ± 4.6	92.2 ± 7.9	96.2 ± 4.7	91.0 ± 6.4	81.7 ± 10.7
Middle slice	92.4 ± 10.6	92.9 ± 8.4	86.1 ± 12.1	77.9 ± 7.6	86.9 ± 8.8	87.7 ± 9.8	83.2 ± 10.0	78.2 ± 12.4
Lower slice	93.3 ± 6.4	88.7 ± 8.7	85.3 ± 11.4	69.9 ± 7.3	78.2 ± 11.2	86.3 ± 8.3	88.7 ± 7.3	86.0 ± 9.5

Segments are numbered in order from septal (1,2), anterior (4,5) to lateral wall (7,8). Values are mean ± s.d. Statistical probabilities were determined by analysis of variance. Values in all segments were significantly different ($p < 0.001$). *: $p < 0.05$, **: $p < 0.01$, ***: $p < 0.001$.

TABLE 2B
The Percent ES Count in Normal Control (%)

Slice/segment	1	2	3	4	5	6	7	8
Upper slice	129.8 ± 7.3	131.2 ± 10.0	130.2 ± 12.1	128.2 ± 12.2	133.3 ± 10.4	140.3 ± 10.4	143.8 ± 7.4	138.3 ± 5.1
Middle slice	128.4 ± 12.2	131.6 ± 9.6	127.6 ± 14.7	125.4 ± 8.3	130.3 ± 10.4	133.6 ± 12.1	133.0 ± 6.9	126.3 ± 9.7
			No significant differences					
Lower slice	123.9 ± 11.4	127.6 ± 10.9	125.6 ± 14.8	120.1 ± 13.7	120.8 ± 12.2	127.6 ± 12.2	127.2 ± 7.4	133.9 ± 9.2

Segments are numbered in order from septal (1, 2), anterior (4, 5) to lateral wall (7, 8). Values are mean ± s.d. Statistical probabilities were determined by analysis of variance. Values in all segments were significantly different ($p < 0.01$). * : $p < 0.05$, ** : $p < 0.01$, *** : $p < 0.001$.

increase in anterolateral wall was significantly lower than that in anterior wall. In the upper and middle slices, the percent count increase in anterolateral wall was significantly lower than that in lateral wall. Thus, the percent count increase tended to be higher at the segments where the percent ED count was relatively low (Fig. 3C, Table 2C).

Count Increase (PET) in Relation to Wall Thickening (MR)

In 80 segments (five cases of normal control), the percent count increase was compared with the percent wall thickening. Images of ECG-gated PET and MR imaging of the same slice of the same case are shown in Fig. 4. The percent count increase ranged from 21% to 100% (mean 56.2%) and the percent wall thickening ranged from 13% to 175% (mean 68.6%). These were correlated well ($r = 0.84$, Fig. 5). In the segments where the percent wall thickening was high, the percent count increase tended to be lower than the percent wall thickening (Fig. 5).

ECG-Gated PET in Patients in Relation to Wall Motion (LVG)

The percent count increase measured by ECG-gated PET was compared with wall motion assessed by LVG

TABLE 2C
The Percent Count Increase in Normal Control (%)

Slice/segment	1	2	3	4	5	6	7	8
Upper slice	39.8 ± 10.1	41.5 ± 7.5	49.5 ± 13.7	51.7 ± 12.6	45.5 ± 18.1	46.2 ± 10.4	59.3 ± 16.1	72.8 ± 26.5
Middle slice	39.8 ± 12.9	42.4 ± 11.4	49.6 ± 16.1	62.1 ± 13.6	50.9 ± 13.9	53.3 ± 16.1	61.3 ± 15.0	66.1 ± 17.2
Lower slice	32.9 ± 7.2	44.7 ± 9.6	47.9 ± 11.9	72.6 ± 21.4	56.0 ± 16.5	48.7 ± 15.0	44.7 ± 17.0	57.2 ± 16.7

Segments are numbered in order from septal (1, 2), anterior (4, 5) to lateral wall (7, 8). Values are mean ± s.d. Statistical probabilities were determined by analysis of variance. Values in all segments were significantly different ($p < 0.001$). * : $p < 0.05$. ** : $p < 0.01$, *** : $p < 0.001$.

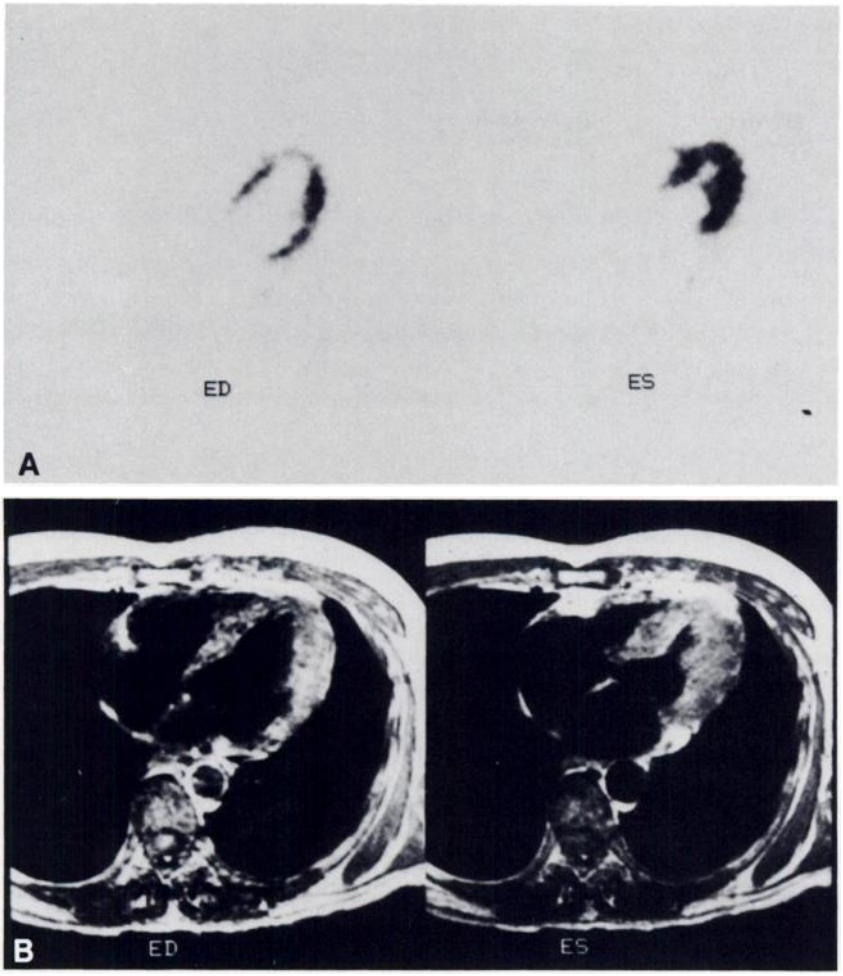

FIGURE 4
Corresponding slice of PET (A) and MR imaging (B) are shown. These images show count distribution in PET reflects wall thickening in MR imaging.

in each corresponding segment. Figure 6 shows the results of Patient 5 in Table 1; the percent count increase reduced in the segments with abnormal wall motion.

Anterobasal segment (Fig. 7A). The percent count increase was 48.6 ± 15.2% in normal control. In patients with CAD, it was 39.1 ± 16.2% in normal wall motion and 14.5 ± 12.4% in reduced wall motion ($p < 0.001$ vs. normal control and $p < 0.01$ vs. normal wall motion).

Anterolateral segment (Fig. 7B). The percent count increase was 55.9 ± 14.8% in normal control. In patients with CAD, it was 43.0 ± 16.4% in normal wall motion, 35.9 ± 14.1% in reduced wall motion ($p < 0.001$ vs. normal control), 8.5 ± 5.2% in akinesis ($p < 0.001$ vs. normal control, $p < 0.001$ vs. normal wall motion and $p < 0.001$ vs. reduced wall motion) and 16.0 ± 29.7% in dyskinesis ($p < 0.001$ vs. normal control). These values significantly decreased as the wall motion worsened.

Apical segment (Fig. 7C). The percent count increase was 64.3 ± 20.4% in normal control. In patients with CAD, it was 38.3 ± 22.8% in normal wall motion ($p < 0.05$ vs. normal control), 32.8 ± 13.4% in reduced wall motion ($p < 0.001$ vs. normal control), 22.5 ± 15.3% in akinesis ($p < 0.001$ vs. normal control) and 10.5 ± 15.5% in dyskinesis ($p < 0.001$ vs. normal control and $p < 0.01$ vs. reduced wall motion). These values significantly decreased as the wall motion worsened.

Posterobasal segments (Fig. 7D). The posterior wall (P_1, P_2) was identified in 13 cases (at middle slice in two cases, at lower slice in 11 cases) in patients with CAD. The percent count increase was 55.4 ± 15.0% in normal control. In patients with CAD, it was 50.4 ± 13.3% in normal wall motion, 23.3 ± 6.0% in reduced wall motion ($p < 0.001$ vs. normal control, $p < 0.001$ vs. normal wall motion) and 13.2 ± 13.3% in akinesis ($p < 0.001$ vs. normal control, $p < 0.001$ vs. normal wall motion). These values significantly decreased as the wall motion worsened.

Septal segment (Fig. 7E). The percent count increase was 41.7 ± 11.5% in normal control. In patients with CAD, it was 29.0 ± 8.5% in normal wall motion, 21.9 ± 9.4% in reduced wall motion ($p < 0.001$ vs. normal control), 21.6 ± 16.1% in akinesis ($p < 0.01$ vs. normal control) and 21.0 ± 11.3% in dyskinesis ($p < 0.001$ vs. normal control). In this segment, these values in patients with CAD did not correlate with the wall motion

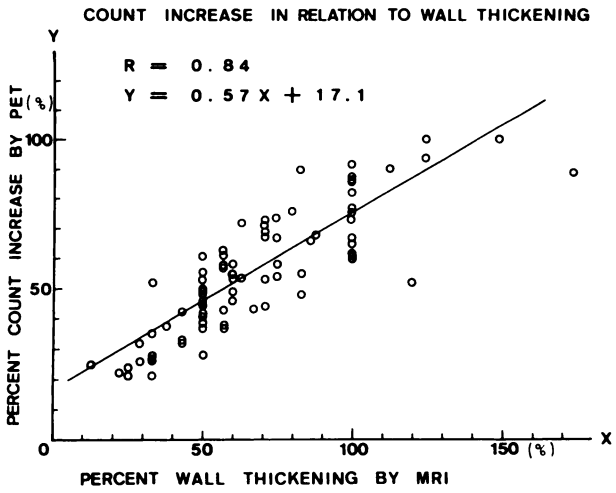

FIGURE 5
Correlation between systolic count increase of PET and systolic wall thickening of MR imaging in 5 normal persons. These correlated well but count increase tends to be smaller than wall thickening especially in segments with high percent wall thickening.

of LVG. In ECG-gated PET, septal wall often preserved good wall thickening even in the case where akinesis or dyskinesis was seen (Fig. 5).

Posterolateral segment (Fig. 7F). The percent count increase was 63.7 ± 15.8% in normal control. In patients with CAD, it was 50.5 ± 16.6% in normal wall motion ($p < 0.05$ vs. normal control), 39.5 ± 11.0% in reduced wall motion ($p < 0.01$ vs. normal control) and 30.9 ± 17.1% in akinesis ($p < 0.001$ vs. normal control, $p < 0.01$ vs. normal wall motion). These values significantly decreased as the wall motion worsened.

Inter- and Intra-Observer Variability in Analysis of the Percent Count Increase in ECG-Gated PET

In normal control, inter- and intraobserver variability was 2.8% and 1.3%, respectively. In patients with CAD, inter- and intraobserver variability was 5.0% and 2.9%, respectively.

DISCUSSION

Left ventricular wall thickening is one of the best indicators of regional LV function, which has been analyzed by echocardiography (*19–25*), LVG (*26–28*), ECG-gated computed tomography (*29–33*) and ECG-gated MRI (*34–36*). In the field of nuclear medicine, regional wall motion has been evaluated by ECG-gated blood-pool imaging (*37–41*), and static myocardial perfusion has been evaluated by thallium-201 (^{201}TI) study (*42–49*). However, regional wall thickening is difficult to assess due to inadequate count density of ^{201}TI. On the other hand, PET has high count efficiency which enables gated acquisition without loss of image quality (*14*). However, quantitative analysis of systolic count increase by ECG-gated PET has been only performed in an animal study (*16*). We think that this method can be applied in the study of humans. In addition, three-dimensional assessment can be performed with tomographic display in ECG-gated PET.

As compared with other imaging techniques, nuclear medicine often applies the nongeometric (count-based) method for assessing volume changes (*38,40,41*). When the object size is smaller than twice that of the spatial resolution in FWHM, the count recovery is related to the object size (*15*). Based on this principle of partial volume effect, the count in the myocardium correlated well with the wall thickness when the actual tracer concentration is constant and the wall thickness is less than twice that of the resolution in FWHM. The effective resolution in FWHM of our PET system is 9 mm in tangential direction and 12 mm in axial direction (*17*). The LV wall thickness is usually <20 mm (*34–*

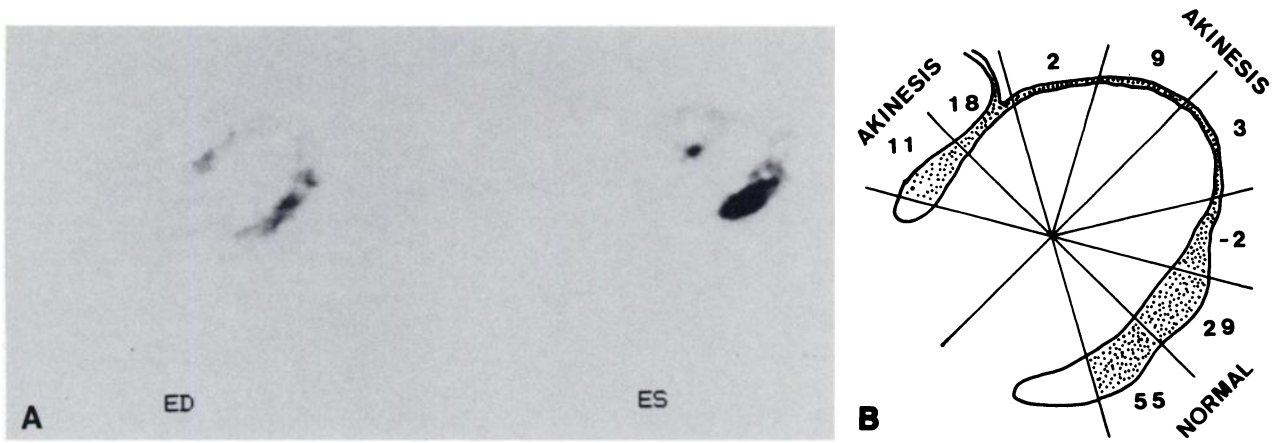

FIGURE 6
ED and ES images (A) at middle slice of Patient 5 of Table 1. This patient has anteroseptal myocardial infarction and systolic wall thickening decreased in these segments. The calculated percent count increase reflects wall thickening even in the segments with anteroseptal myocardial infarction where count of myocardium decreased (B).

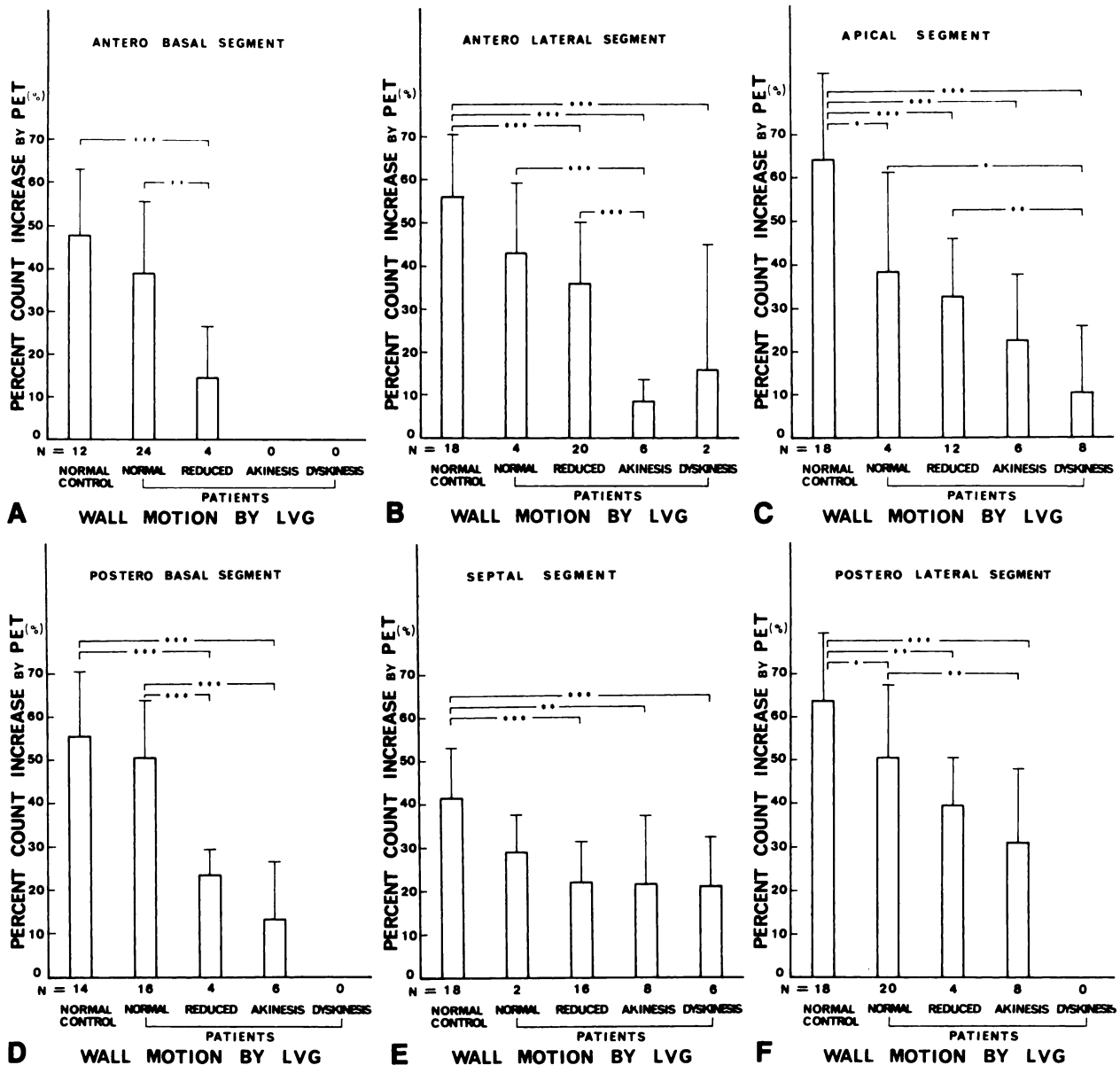

FIGURE 7

Comparison between ECG-gated positron tomography and biplane left ventriculography in 16 patients with significant coronary disease. Values are mean ± s.d. Analysis was performed by the segment as anterobasal (A), anterolateral (B), apical (C), posterobasal (D), septal (E) and posterolateral segment (F). The percent count increase significantly decreased as the wall motion worsened. In addition, the percent count increase in normal control tended to be lower than that in normal wall motion in coronary patients. Statistical probabilities were determined by the paired t-test; *: $p < 0.05$, **: $p < 0.01$, ***: $p < 0.001$.

36) and is within the resolution of our PET system. Therefore, our PET system should underestimate the actual concentration of the tracer within LV myocardium depending on its thickness particularly in ED. Thus, the percent count increase from ED to ES was considered to represent regional wall thickening. This nongeometric method may be applied with most clinical PET devices with the spatial resolution as same or less than ours, unless the patient has severe LV hypertrophy.

The percent count increase assessed by ECG-gated PET correlated well with the percent wall thickening assessed by MRI. The percent count increase tended to be lower than the percent wall thickening especially in the segments where the percent wall thickening was high (≧50%). This may suggest that count rates recovered from myocardium depend upon regional myocardial wall thickness in a nonlinear fashion; greater underestimation of regional count may occur in thick myocardial wall. In the segments with high percent count increase (≧50%; this is often encountered in normal segments), this underestimation of the percent

count increase should be considered. This may explain the large differences in regional percent count increase of normal controls.

In normal controls, the percent count increase was significantly different among various segments even in the same slice. In the previous study MRI (*34*), it was shown that the percent wall thickening in anterior wall was the highest and significantly higher than that in septal wall in normal subjects. This suggests that count increase or wall thickening of LV wall should be evaluated separately in each segment or may require standardization by each normal value.

In patients with CAD, the percent count increase assessed by PET correlated well with the wall motion score assessed by LVG in each segment, indicating the percent count increase as a reliable index of regional wall motion. In septal wall, however, the percent count increase did not correlate with the wall motion abnormality assessed by LVG. This is partly due to the fact that LVG using projection images cannot always separate normal septal wall from abnormal (akinesis or dyskinesis) anteroseptal wall, while ECG-gated PET can do so using a tomographic display (Fig. 8). In addition, regional wall thickening and regional wall excursion are different phenomena, although both of them are good indicators of regional myocardial function.

Interestingly, the percent count increase in normal controls tend to be higher than that in visually normal wall motion in patients with CAD. It may be partly due to the fact that changes of LV geometry or dialation may occur in the patients with CAD and may influence the percent count increase. However, in patients with CAD, the percent count increase assessed by ECG-gated PET may delineate minimal wall motion abnormality which qualitative analysis of LVG cannot detect.

In this method, analysis is performed automatically except for decision of the middle slice and the center point in each slice, therefore, high reproducibility can be obtained.

The major limitation of this method is that it uses transverse slices. Inferior wall cannot be analyzed exactly because it is usually oblique to the transverse section and sometimes nearly parallel to that. In addition, the count may be overestimated because the transaxial section is not completely perpendicular to LV wall (*34,35*). These problems may be partly overcome by selecting control slices of the myocardium and setting a normal range by the segment of each slice. In addition, change in the orientation of the LV wall relative to imaging plane from ED to ES may influence the analysis of systolic count increase (*50*). This change of orientation is probably variable and it is different in a well-contracting heart (normal case) and in a poorly contracting one (myocardial infarction). These limitations should be considered in analysis of percent count increase. A true three-dimensional assessment using cardiac short and long axis section (*51*) may be needed in the future.

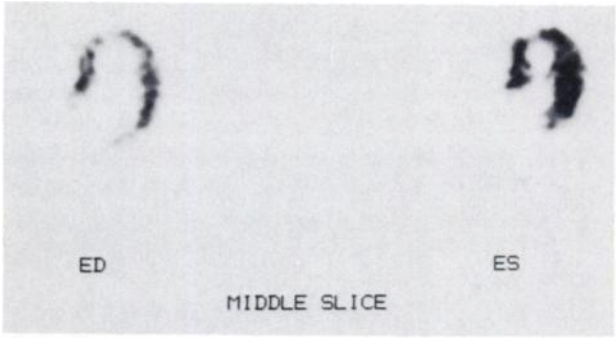

FIGURE 8
ECG-gated PET images of the middle slice in Patient 13 of Table 1. Septal wall was akinetic on left ventriculography. However, septal wall preserved good wall thickening on ECG-gated positron tomography.

The percent count increase was relatively high as compared with other reports. This is mainly due to overestimation of the count in the thicker ES myocardium in X-Y as well as Z axis directions than in ED myocardium. In addition, the value was also high in the segments with severe wall motion abnormality. The percent count increase is calculated by averaging five points of each segment. When two or three points have poor systolic count increase but others have relatively good systolic count increase, regional percent count increase is relatively high. It may fail to identify subtle wall motion abnormality in small infarct.

On the other hand, count statistics are improved by averaging five points in each segment, which is helpful in analysis of severe myocardial infarction where decrease of count may impair count statistics (Fig. 6). However, this problem is one of the limitations of this method and analysis of severe myocardial infarction should be performed carefully.

The percent count increase in dyskinesis tended to be smaller than that in akinesis (Fig. 7). It would be of interest to know whether systolic count increase in dyskinesis is smaller than that in akinesis, however, it is difficult to prove statistically due to low count noise ratio in severe infarction.

The standard deviation in segments with various wall motion is relatively large. The reasons are as follows: Segments of transverse images of PET do not completely correpond to those of RAO and LAO images of LVG. In addition, systolic count increase by PET was evaluated using tomographic images; wall motion LVG using projection images. Therefore, site of decreased count increase by PET may not always correspond to that of abnormal wall motion by LVG.

PET is useful for analysis of myocardial perfusion and metabolism (*1–14*). If quantitative analysis of myocardial systolic wall thickening can be performed by ECG-gated PET, the combined analysis of LV wall

thickening, perfusion and metabolism can be done. In the future, relationships between wall thickening, perfusion and metabolism will be analyzed more precisely in detail.

In conclusion, ECG-gated PET enables quantitative analysis of regional wall motion using the percent count increase. Normal value of the percent count increase was defined and its reliability was evaluated by comparison with the wall motion of LVG in patients with CAD.

ACKNOWLEDGMENT

The authors thank Tetsuro Fudo, MD and Toru Fujita, RT for their medical and technical assistance.

REFERENCES

1. Brunken R, Tillisch J, Schwaiger M, et al. Regional perfusion, glucose metabolism and wall motion in patients with chronic electrographic Q wave infarctions: evidence for persistence of viable tissue in some infarct regions by positron emission tomography. *Circulation* 1986; 73:951–963.
2. Schelbert HR, Phelps ME, Huang SC, et al. N-13 ammonia as an indicator of myocardial blood flow. *Circulation* 1981; 63:1259–1272.
3. Bergmann SR, Fox KA, Rand AL, et al. Quantification of regional myocardial blood flow in vivo with $H_2{}^{15}O$. *Circulation* 1984; 70:724–733.
4. Gould KL, Goldstein RA, Mullani NA, et al. Noninvasive assessment of coronary stenosis by myocardial perfusion imaging during pharmacologic coronary vasodilation. VIII. Clinical feasibility of positron cardiac imaging without cyclotron using generator-produced rubidium-82. *J Am Coll Cardiol* 1986; 7:775–789.
5. Marshall RC, Tillisch JH, Phelps ME, et al. Identification and differenciation of resting myocardial ischemia and infarction in man with positron computed tomography, ^{18}F-labeled fluorodeoxyglucose and N-13 ammonia. *Circulation* 1983; 67:766–778.
6. Yonekura Y, Tamaki N, Senda M, et al. Detection of coronary artery disease with ^{13}N-ammonia and high-resolution positron emission computed tomography. *Am Heart J* 1987; 113:645–654.
7. Tamaki N, Yonekura Y, Senda M, et al. Myocardial positron computed tomography with ^{13}N-ammonia at rest and during exercise. *Eur J Nucl Med* 1985; 11:246–251.
8. Goldstein RA, Kirkeeide RL, Smalling RW, et al. Changes in myocardial perfusion reserve after PTCA: noninvasive assessment with positron tomography. *J Nucl Med* 1987; 28:1262–1267.
9. Ratib O, Phelps ME, Huang SC, Henze E, Selin CE, Schelbert HR. Positron tomography with deoxyglucose for estimating local myocardial glucose metabolism. *J Nucl Med* 1982; 23:577–586.
10. Schwaiger M, Schelbert HR, Ellison D, et al. Sustained regional abnormalities in cardiac metabolism after transient ischemia in the chronic dog model. *J Am Coll Cardiol* 1985; 6:336–347.
11. Brunken R, Schwaiger M, Grover-Mckay M, Phelps ME, Tillisch J, Schelbert HR. Positron emission tomography detects tissue metabolic activity in myocardial segments with persistent thallium perfusion defects. *J Am Coll Cardiol* 1987; 10:557–567.
12. Schwaiger M, Brunken R, Grover-Mckay M, et al. Regional myocardial metabolism in patients with acute myocardial infarction assessed by positron emission tomography. *J Am Coll Cardiol* 1986; 8:800–808.
13. Yonekura Y, Brill AB, Som P, et al. Regional myocardial substrate uptake in hypertensive rats: a quantitative auto-radiographic measurement. *Science* 1985; 227:1494–1496.
14. Hoffman EJ, Phelps ME, Wisenberg G, Schelbert HR, Kuhl DE. Electrographic gating in positron emission computed tomography. *J Comput Assist Tomogr* 1979; 3:733–739.
15. Hoffman EJ, Huang SC, Phelps ME. Quantitation in positron emission computed tomography: 1. effect of object size. *J Comput Assist Tomogr* 1979; 3:299–308.
16. Wisenberg G, Schelbert HR, Hoffman EJ, et al. In vivo quantification of myocardial blood flow by positron-emission computed tomography. *Circulation* 1981; 63:1248–1258.
17. Senda M, Tamaki N, Yonekura Y, et al. Performance characteristics of positologica III, a whole body positron emission tomograph. *J Comput Assist Tomogr* 1985; 9:940–946.
18. Austine WG, Edwards JE, Frye RL, et al. A reporting system on patients evaluated for coronary artery disease. (AHA committee report). *Circulation* 1975; 51:5.
19. St. John Sutton MG, Tajik AJ, Gibson DG, Brown DJ, Seward JB, Guiliani ER. Echocardiographic assessment of left ventricular filling and septal and posterior wall dynamics in idiopathic subaortic stenosis. *Circulation* 1978; 57:512–520.
20. Corya BC, Feigenbaum H, Rasmussen S, Black MJ. Echocardiographic features of conjestive cardiomyopathy compared with normal subjects and patients with coronary artery disease. *Circulation* 1974; 49: 1153–1159.
21. Morganroth J, Kerber RE, Abboud FM. Echocardiographic detection of regional myocardial infarction. *Circulation* 1973; 49:997–1005.
22. Visser CA, Lie KI, Kan G, Meltzer R, Durrer D. Detection and quantification of acute, isolated myocardial infarction by two dimensional echocardiography. *Am J Cardiol* 1981; 47:1020–1025.
23. Heger IJ, Weyman AE, Wann LS, Rogers EW, Dillon JC, Feigenbaum H. Cross-sectional echocardiographic analysis of the extent of left ventricular asynergy in acute myocardial infarction. *Circulation* 1980; 61: 1113–1118.
24. Maron BJ, Gottdiener JS, Bonow RO, Epstein SE. Hypertrophic cardiomyopathy with unusual location of left ventricular hypertrophy undetectable by M-mode echocardiography. *Circulation* 1981; 63:409–418.
25. Goldberg SJ, Hutter IJ, Feldman L, Goldberg SM. Two sensitive echocardiographic techniques for detecting doxorubicin toxicity. *Med Pediatr Oncol* 1983; 11:172–177.
26. Eber LM, Greenberg HM, Cooke JM, Gorlin R. Dynamic changes in left ventricular free wall thickness in the human heart. *Circulation* 1969; 39:455–464.
27. Hugenholtz PG, Kaplan E, Hull E. Determination of left ventricular wall thickness by angiocardiography. *Am Heart J* 1969; 78:513–522.
28. Croxson RS, Raphael MJ. Angiographic assessment of congestive cardiomyopathy. *Br Heart J* 1969; 31:390–391.
29. Mattrey RF, Higgins CB. Detection of regional myocardial dysfunction during ischemia with computer-

ized tomography documentation and physiologic basis. *Invest Radiol* 1982; 17:329–335.
30. Mattrey RF, Long SA, Erickson SW, Higgins CB. Computer technique for monitoring time-dependent changes from sequencial CT images. *J Comput Assist Tomogr* 1983; 7:379–382.
31. Slutsky RA, Mattrey RF, Long SA, Higgins CB. In vivo estimation of myocardial infarct size and left ventricular function by prospectively gated computerized transmission tomography. *Circulation* 1983; 67:759–765.
32. Lackner K, Thum P. Computed tomography of the heart: ECG-gated and continuous scans. *Radiology* 1981; 140:413–420.
33. Mattrey TR, Slutsky RA, Long SA, Higgins CB. In vivo assessment of left ventricular wall and chamber dynamics during transient myocardial ischemia using prospectively ECG-gated computerized transmission tomography. *Circulation* 1983; 67:1245–1251.
34. Fisher MR, von Schulthess GK, Higgins CB. Multiphasic cardiac magnetic resonance imaging: normal regional left ventricular wall thickening. *Am J Radiol* 1985; 145:27–30.
35. Sechtem U, Sommerhoff BA, Markiewicz W, et al. Regional left ventricular wall thickening by magnetic resonance imaging: evaluation in normal persons and patients with global and regional dysfunction. *Am J Cardiol* 1987; 59:141–145.
36. Akins EW, Hill JA, Sievers KW, Conti CR. Assessment of left ventricular wall thickness in healed myocardial infarction by magnetic resonance imaging. *Am J Cardiol* 1987; 59:24–28.
37. Yamashita K, Tanaka M, Asada N, et al. A new method of three dimensional analysis of left ventricular wall motion. *Eur J Nucl Med* 1988; 14:113–119.
38. Maddox DE, Holman BL, Whnne J, Wagner HN Jr. Ejection fraction image: a noninvasive index of regional left ventricular wall motion. *Am J Cardiol* 1978; 141:1230–1238.
39. Nakajima K, Bunko H, Tonami N, Tada A, Hisada K. Quantification of segmental wall motion by length-based Fourier analysis. *J Nucl Med* 1984; 25:917–921.
40. Tamaki N, Mukai T, Ishii Y, et al. Multiaxial tomography of heart chambers by gated blood pool emission computed tomography using a rotating gamma camera. *Radiology* 1983; 147:545–554.
41. Underwood SR, Walton S, Ell PJ, Jarritt PH, Emannel RW, Swanton RH. Gated blood pool emission tomography: a new technique for the investigation of cardiac structure and function. *Eur J Nucl Med* 1985; 10:332–337.
42. Strauss HW, Harrison K, Langan JK, Lebowitz E, Pitt B. Thallium-201 for myocardial imaging: relation of thallium-201 to regional myocardial perfusion. *Circulation* 1976; 51:641–654.
43. Ritchie JL, Trobaugh GB, Hamilton GW, et al. Myocardial imaging with thallium-201 at rest and during exercise: comparison with coronary arteriography and resting and stress electerocardiography. *Circulation* 1977; 56:66–71.
44. Botvinick EH, Taradesh MR, Hames DM, Parmley WW. Thallium-201 myocardial perfusion scintigraphy for the clinical classification of normal, abnormal and equivocal electrocardiographic stress tests. *Am J Cardiol* 1978; 41:41–51.
45. Pohost GM, Zir LM, Moore RH, McKusick KA, Guiney TE, Beller GA. Differentiation of transiently ischemic from infarcted myocardium by serial imaging after a single dose of thallium-201. *Circulation* 1977; 55:294–302.
46. Rozanski A, Berman DS, Gray R, et al. Use of thallium-201 redistribution scintigraphy in the preoperative differentiation of reversible and nonreversible myocardial asynergy. *Circulation* 1981; 64:936–944.
47. Beller GA, Watson DD, Ackell P, Pohost GM. Time course of thallium-201 redistribution after transient myocardial ischemia. *Circulation* 1980; 61:791–797.
48. Berger BC, Watson DD, Burwell LR, et al. Redistribution of thallium at rest in patients with stable and unstable angina and the effect of coronary artery bypass srugery. *Circulation* 1979; 60:1114–1125.
49. Garcia E, Maddahi J, Berman D, et al. Space/time quantitation of thallium-201 myocardial scintigraphy. *J Nucl Med* 1981; 22:309.
50. White CW, Wilson RF, Marcus ML. Methods of measuring myocardial blood flow in humans. *Prog Cardiovasc Dis* 1988; 31:79–94.
51. Senda M, Yonekura Y, Tamaki N, et al. Interpolating and oblique-angle tomograms in myocardial PET using nitrogen-13 ammonia. *J Nucl Med* 1986; 27: 1830–1836.